



Five-Hole Flow Angle Probe Calibration for the NASA Glenn Icing Research Tunnel

Jose C. Gonzalez and E. Allen Arrington
Dynacs Engineering Company, Inc., Brook Park, Ohio

Prepared for the
19th Advanced Measurement and Ground Testing Technology Conference
sponsored by the American Institute of Aeronautics and Astronautics
New Orleans, Louisiana, June 17-20, 1996

Prepared under Contract NAS3-27186

National Aeronautics and
Space Administration

Glenn Research Center

Acknowledgments

The authors wish to thank Masashi Mizukami, formerly of the NASA Glenn Research Center, for his computer programming assistance with the multiple regression model.

Available from

NASA Center for Aerospace Information
7121 Standard Drive
Hanover, MD 21076
Price Code: A03

National Technical Information Service
5285 Port Royal Road
Springfield, VA 22100
Price Code: A03

FIVE-HOLE FLOW ANGLE PROBE CALIBRATION FOR THE NASA GLENN ICING RESEARCH TUNNEL

Jose C. Gonzalez and E. Allen Arrington
DYNACS Engineering Co., Inc.
Brook Park, Ohio 44142

SUMMARY

A spring 1997 test section calibration program is scheduled for the NASA Glenn Research Center Icing Research Tunnel following the installation of new water injecting spray bars. A set of new five-hole flow angle pressure probes was fabricated to properly calibrate the test section for total pressure, static pressure, and flow angle. The probes have nine pressure ports: five total pressure ports on a hemispherical head and four static pressure ports located 14.7 diameters downstream of the head. The probes were calibrated in the NASA Glenn 3.5-in.-diameter free-jet calibration facility. After completing calibration data acquisition for two probes, two data prediction models were evaluated. Prediction errors from a linear discrete model proved to be no worse than those from a full third-order multiple regression model. The linear discrete model only required calibration data acquisition according to an abridged test matrix, thus saving considerable time and financial resources over the multiple regression model that required calibration data acquisition according to a more extensive test matrix. Uncertainties in calibration coefficients and predicted values of flow angle, total pressure, static pressure, Mach number, and velocity were examined. These uncertainties consider the instrumentation that will be available in the Icing Research Tunnel for future test section calibration testing.

SYMBOLS

b	curve fit intercept for flow angle coefficient versus probe angle data
C_M	compressibility coefficient
C_o	total pressure coefficient
$C_{o,avg}$	average total pressure coefficient used by discrete linear model
C_q	dynamic pressure coefficient
$C_{q,avg}$	average dynamic pressure coefficient used by the discrete linear model
C_α	pitch angle pressure coefficient
C_β	yaw angle pressure coefficient
D	diameter, in.
K	coefficient or constant in data prediction models
M_{jet}	calibration jet Mach number computed with $P_{T,plenum}$ and $P_{S,room}$
M_{probe}	probe Mach number computed with P_5 and $P_{6-9,avg}$
M_{local}	local Mach number computed with $P_{T,local}$ and $P_{S,local}$
m	curve fit slope for flow angle coefficient versus probe angle data, 1/deg

N	number of data points
P	pressure, psia
$P_{i=1 \text{ to } 9}$	probe pressures, psia
$P_{1-4,avg}$	$(P_1+P_2+P_3+P_4)/4$
$P_{6-9,avg}$	$(P_6+P_7+P_8+P_9)/4$
R	specific gas constant for air, $\text{ft}^2/(\text{sec}^2 \text{ } ^\circ\text{R})$
$S_{\alpha,C\alpha}$	standard error of the estimate for α calibration data and the predicted α data, deg
$S_{C\alpha}$	standard deviation of the calibration C_α data, deg
SSD	sum of the squared differences between calibration data and calibration data mean
SSE	sum of the squared errors between calibration data and model data predictions
T	temperature, $^\circ\text{R}$
t	value from a statistical t-distribution
V	velocity, ft/sec
X	jet/probe centerline longitudinal coordinate with origin at jet exit, in.
Y	jet/probe horizontal (yaw plane) coordinate with origin at jet exit center, in.
Z	jet/probe vertical (pitch plane) coordinate with origin at jet exit center, in.
α	pitch angle of attack, deg
α_F	calibration jet flow angle in pitch plane, deg
α_P	probe bias angle in pitch plane (also equal to $K_{0,\alpha}$), degrees
β	yaw angle of attack, deg
β_F	calibration jet flow angle in yaw plane, deg
β_P	probe bias angle in yaw plane (also equal to $K_{0,\beta}$), deg
ϕ	probe roll angle, deg
γ	ratio of specific heats for air

Subscripts:

avg	average
I	inverted probe roll orientation ($\phi = 180^\circ$)

jet	pertaining to the calibration jet flow field
local	local free-stream conditions of CE-12 jet or Icing Research Tunnel test section
N	normal probe roll orientation ($\phi = 0^\circ$)
plenum	pertaining to CE-12 jet plenum
probe	pertaining to five-hole probes
room	pertaining to CE-12 calibration test cell
S	static conditions
T	total or stagnation conditions
α	pertaining to pitch angle
β	pertaining to yaw angle
0 to 19	coefficient number

INTRODUCTION

During the fall and winter of 1996, the NASA Glenn Research Center Icing Research Tunnel (IRT) underwent some facility enhancements. More specifically, the spray bars used to inject water into the air stream were replaced with more aerodynamic spray bars. In 1999 there are even plans to replace the current IRT heat exchanger with one that is more aerodynamic. To gauge the improvement in flow quality and to calibrate the IRT test section following these and any other major tunnel modifications, a survey rake with carefully calibrated probes was needed. A vertical calibration/survey rake already existed, but it had probes that were poorly designed and constructed. In addition, the vertical rake design did not lend itself to easy alignment with respect to the test section centerline. As a result of these deficiencies, new hardware was designed and fabricated. Twelve five-hole flow angle pressure probes and a 9-ft horizontal rake body were built. Before the new probes could be used to calibrate and quantify the flow quality in the IRT test section, they had to be individually calibrated for total pressure, static pressure, and flow angle. The focus of this report will be the probe calibration test program and subsequent data reduction. The specific objectives are given below.

1. Briefly describe the geometrical features of the IRT five-hole probes and the NASA Glenn 3.5-in.-diameter free-jet calibration facility.
2. Present general trends for the experimental calibration data.
3. Evaluate and compare the errors associated with using a discrete linear data prediction model (which requires calibration data acquired according to an abridged or sparse test matrix) and a full third-order multiple regression data prediction model (which requires calibration data acquired according to an unabridged or full test matrix).
4. Present calibration coefficients for the data prediction model that has the more favorable comparison.
5. Present uncertainties in the calibration coefficients and uncertainties in predicted flow angle, total pressure, static pressure, Mach number, and velocity.

FIVE-HOLE PROBE DESCRIPTION

Figure 1 shows the five-hole probe design, pressure port layout, and pertinent probe nomenclature such as probe roll angle ϕ , probe pitch angle of attack α , probe yaw angle of attack β , and jet/probe X,Y,Z-coordinate system. The probe has nine pressure ports: five total pressure ports on the hemispherical head and four static pressure ports

14.67 probe diameters downstream of the head. Flow angle pressures P_1 , P_2 , P_3 , and P_4 are sensed by the circumferential ports on the head. Total pressure P_5 is sensed by the center port on the head. Static pressures P_6 , P_7 , P_8 , and P_9 are sensed by the pressure ports downstream of the probe head. The relative measurement locations of $P_{T,plenum}$, $P_{S,room}$, $P_{T,local}$, and $P_{S,local}$ are also defined in figure 1. Each of the 12 probes for the new IRT 9-ft test section survey rake was constructed by brazing tubular components together to form the overall 27.75-in.-length. One 5.75-in.-long tubular section comprised the probe head and the downstream static ports; the remaining 22-in.-long section was a simple probe support tube. The overall straightness of the two individual sections was typically 0.006-in. The brazing process did not always produce perfect results. At this braze joint, angles as large as 0.3° were measured.

CALIBRATION FACILITY DESCRIPTION

Figure 2 is a photograph of the IRT five-hole probe calibration test apparatus in the NASA Glenn 3.5-in.-diameter free-jet calibration facility. This facility is located in test cell CE-12 of the NASA Glenn Engine Research Building and will be referred to as CE-12 herein. The facility consists of a 3.5-in.-diameter free jet that is exhausted into the CE-12 test cell and is vented to the atmosphere via ceiling vents. Flow to the 29.2-in.-diameter plenum tank is supplied through an 8-in.-diameter, 40 psig air line connected to the NASA Glenn central air supply service. Two valves, a 6-in. main ball valve and a 1.5-in. bypass globe valve, throttle the 40-psig air down to the desired plenum stagnation pressure. The plenum tank is fitted with two perforated plates, one honeycomb section, and four turbulence reduction screens which insure good jet flow quality. Also shown in figure 2 is the CE-12 high-accuracy pitch-yaw actuator system, which consists of an 8-in.-diameter rotary pitch table mounted on a 12-in.-diameter rotary yaw table. The 8-in. table lies in the X,Z-pitch plane and the 12-in. table lies in the X,Y-yaw plane. Stepper motors fitted with optical feedback encoders drive the rotary tables to any pitch and yaw angle.

Probes are aligned with respect to the jet axis centerline using the CE-12 alignment fixture, which consists of a flange that attaches to the jet nozzle exit. To this flange, precision squares of varying sizes can be rigidly fastened in either the pitch (X,Z) or yaw (X,Y) planes. Probes are aligned so that the probe support shaft is parallel to the edge of the squares. Figure 3 shows the CE-12 alignment fixture (attached to the jet exit nozzle) being used to align a five-hole probe.

The CE-12 calibration facility is equipped with standard NASA Glenn instrumentation and data acquisition systems: Escort D+ multichannel data acquisition system, multiport electronically scanned pressure system (ESP), and probe actuation and control system (PACS). All three of these systems worked in concert to acquire data during five-hole probe calibration. The ESP system was equipped with a ± 5 -psid pressure module capable of sampling 32 simultaneous pressures.

Before the actual five-hole probe calibration test began, it was necessary to calibrate the CE-12 free jet for total pressure recovery and static pressure recovery because measurements of this type had not been made before. Total pressure recovery was measured by placing a total pressure rake downstream of the jet exit and correlating the measured local total pressures $P_{T,local}$ with the total pressure measured in the plenum $P_{T,plenum}$. The total pressure recovery data are plotted versus jet Mach number in figure 4 for the axial position of $X = 0.571D_{jet}$. This axial station is close to the location where the five-hole probe heads were located during calibration. Only the total pressure measurements made in the center core of the jet are considered (the center 65 percent of the jet cross-sectional area). The curve fit through the data produces a trend that goes above a total pressure recovery of 1.0, which may be the result of the plenum total pressure probe having less than perfect total pressure recovery itself.

The static pressure recovery of the jet was measured with a static pressure probe placed on the jet centerline. The static pressure measured by this probe, $P_{S,local}$, was then correlated with the static pressure measured in the CE-12 test cell, $P_{S,room}$. Figure 5 shows the jet static pressure recovery at $X = 2.286D_{jet}$. This axial position corresponds to the axial location where the five-hole probe static pressure ports were located during calibration. These data indicate increasing local static pressure with increasing jet Mach number, a trend resulting from the localized flow phenomena generated by the jet shear layer entraining surrounding air. As required during five-hole probe data reduction, local total pressure and static pressure were computed using the curve fits in figures 4 and 5.

TEST PROGRAM

Each one of the 12 IRT 5-hole probes was set up in the CE-12 calibration facility (fig. 2). Visible in this photograph is the support arm structure used to hold the five-hole probe in the jet flow. The probe tip was positioned

at $X = 0.714D_{jet}$, which resulted in the static pressure ports being located at $X = 2.286D_{jet}$. The probe shaft holder was positioned 28 probe diameters downstream of the static pressure ports, or at $X = 5.286D_{jet}$. The probe shaft holder has 1- by 1-in. cross-sectional dimensions and has bevels with a 16° leading edge.

The probes were aligned with respect to the jet axis centerline using the CE-12 alignment fixture. The 5.75-in. length of the probe containing the total and static pressure ports was aligned parallel to the alignment fixture squares to within $\pm 0.02^\circ$. Absolute positioning accuracy of the probe shaft centerline with respect to the jet axis centerline was estimated to be $\pm 0.05^\circ$. The remaining length of the probe was allowed to deviate from parallel as dictated by the braze joint misalignment. As previously mentioned, the worst braze joint misalignments were about 0.3° . For this reason, the probe shaft beyond this braze joint could not be used for alignment.

Consideration had to be given to the efficient collection of calibration data because the CE-12 calibration facility could only accommodate one probe at a time. The data collection approach was to follow an unabridged or full test matrix for the first two probes and then assess the possibility of reducing the test matrix by evaluating the errors associated with using two different data prediction models. One of the data prediction models required that calibration data be acquired according to an unabridged or full test matrix whereas the other allowed data to be acquired according to an abridged or sparse test matrix. The unabridged and abridged test matrices are graphically represented in figure 6. The $\pm 5^\circ$ pitch-yaw range in the test matrices was selected because it is anticipated that flow angles within the IRT test section would not exceed this range. Typical flow angles in the IRT test section should be within $\pm 2^\circ$. The Mach number range (0.1 to 0.6) selected for the test matrices matches the IRT test section range. Unfortunately, the exact probe Reynolds numbers anticipated in the IRT test section could not be matched in the CE-12 free jet. The IRT test section is normally run at lower total temperatures, lower total pressures, and lower static pressures. These Reynolds number differences are not expected to have any significant affect on the calibration constants and coefficients. To properly quantify probe bias and jet flow angles, calibration data had to be acquired at two different roll angles: $\phi = 0^\circ$ and $\phi = 180^\circ$. The roll angle of $\phi = 0^\circ$ will be referred to as the normal, or N-roll orientation and the roll angle of $\phi = 180^\circ$ will be referred to as the inverted, or I-roll orientation. By overlaying the calibration curves at these two roll angles, probe bias and jet flow angles could be computed based upon the intersection of the curves.

Data acquired during calibration testing followed the test matrices described in figure 6 and included all nine probe pressures, jet plenum total pressure, CE-12 room static pressure, jet plenum total temperature, pitch angle position, and yaw angle position. Typical values of plenum total pressure ranged between 14.5 and 18.4 psia for the six calibration Mach numbers. CE-12 test cell static pressure always remained around 14.4 psia. Plenum total temperature was consistently about 530 °R. For every data point recorded, twenty 1-sec data scans were collected and averaged. For a number of probes, multiple data points were collected to assess repeatability and to aid in the computation of some uncertainties.

DATA REDUCTION

Third-order multiple regression model.—Two data prediction models were being considered at the start of the calibration program. The first was a full third-order multiple regression model with three independent variables, C_α , C_β , and C_M that would predict four different dependent variables (α , β , C_o , or C_q) depending on the coefficient set selected. The pitch and yaw angle pressure coefficients are C_α and C_β , respectively and are defined as:

$$C_\alpha = \frac{(P_3 - P_1)}{(P_5 - P_{1-4,avg})} \quad (1)$$

$$C_\beta = \frac{(P_4 - P_2)}{(P_5 - P_{1-4,avg})} \quad (2)$$

These pressure coefficients exhibit very linear behavior with flow angle since the numerator measures the differential pressure across opposing pressure ports in either the pitch or yaw plane. The denominator, an approximation of the probe dynamic pressure, serves to nondimensionalize the coefficients. Reference 1 showed that the definitions of C_α and C_β given here are optimal for five-hole probe calibration since the slopes of calibration curves derived from C_α and C_β exhibit minimal change.

The compressibility coefficient C_M , used in the multiple regression model, represents the approximate probe dynamic pressure nondimensionalized by the total pressure and is defined as

$$C_M = \frac{(P_5 - P_{1-4,avg})}{P_5} \quad (3)$$

The multiple regression model does predict α and β explicitly but predicts total pressure and static pressure implicitly via a total pressure coefficient C_o and a dynamic pressure coefficient C_q , which are defined as

$$C_o = \frac{(P_5 - P_{T,local})}{(P_5 - P_{6-9,avg})} \quad (4)$$

$$C_q = \frac{(P_5 - P_{6-9,avg})}{(P_{T,local} - P_{S,local})} \quad (5)$$

The actual data prediction equations for the multiple regression model are defined (some of the equations have been abbreviated for brevity) as

$$\begin{aligned} \alpha = & K_{0,\alpha} + K_{1,\alpha}C_\alpha + K_{2,\alpha}C_\beta + K_{3,\alpha}C_M + K_{4,\alpha}C_\alpha^2 + K_{5,\alpha}C_\beta^2 + K_{6,\alpha}C_M^2 + K_{7,\alpha}C_\alpha C_\beta \\ & + K_{8,\alpha}C_\alpha C_M + K_{9,\alpha}C_\beta C_M + K_{10,\alpha}C_\alpha^3 + K_{11,\alpha}C_\beta^3 + K_{12,\alpha}C_M^3 \\ & + K_{13,\alpha}C_\alpha^2 C_\beta + K_{14,\alpha}C_\alpha C_M^2 + K_{15,\alpha}C_\beta^2 C_\alpha + K_{16,\alpha}C_\beta^2 C_M + K_{17,\alpha}C_M^2 C_\alpha \\ & + K_{18,\alpha}C_M^2 C_\beta + K_{19,\alpha}C_\alpha C_\beta C_M \end{aligned} \quad (6)$$

$$\beta = K_{0,\beta} + K_{1,\beta}C_\alpha + K_{2,\beta}C_\beta + K_{3,\beta}C_M + K_{4,\beta}C_\alpha^2 + \dots + K_{19,\beta}C_\alpha C_\beta C_M \quad (7)$$

$$C_o = K_{0,C_o} + K_{1,C_o}C_\alpha + K_{2,C_o}C_\beta + K_{3,C_o}C_M + K_{4,C_o}C_\alpha^2 + \dots + K_{19,C_o}C_\alpha C_\beta C_M \quad (8)$$

$$C_q = K_{0,C_q} + K_{1,C_q}C_\alpha + K_{2,C_q}C_\beta + K_{3,C_q}C_M + K_{4,C_q}C_\alpha^2 + \dots + K_{19,C_q}C_\alpha C_\beta C_M \quad (9)$$

Coefficient generation for this model requires calibration data acquired according to the unabridged test matrix and a least-squares curve-fitting technique employing matrix algebra. The matrix algebra required to determine the calibration coefficients is

$$[K] = [C^T C]^{-1} [C]^T [A] \quad (10)$$

where $[K]$ is the 20×1 column vector containing the calibration coefficients; $[C]$ is the $N \times 20$ matrix containing the flow angle pressure and compressibility coefficient terms (i.e., 1, C_α , C_β , C_M , C_α^2 , ..., and $C_\alpha C_\beta C_M$); $[A]$ is the $N \times 1$ column vector containing the flow property under consideration and evaluated using data from calibration (α , β , C_o , or C_q); and N is the total number of calibration data points. Note that each row in the $[C]$ and $[A]$ matrices corresponds to a data point in the unabridged calibration test matrix at $\phi = 0^\circ$. This matrix algebra procedure must be carried out four times to generate calibration coefficients for each of the four flow properties (α , β , C_o , and C_q). Reference 2 provides more details about this particular multiple regression model.

Discrete linear model.—The multiple regression model would have required extensive calibration data acquisition at considerable cost in terms of time and money. For this reason, a second data prediction model was considered. This second model consists of discrete linear models for each calibration Mach number in terms of α , β ,

C_o , and C_q . Specific sets of constants and coefficients are defined for every calibration Mach number. Linear interpolation is used for Mach numbers other than those set during calibration. Calibration data for this model can be acquired according to the abridged test matrix seen in figure 6. The model is described as

$$\alpha = K_{0,\alpha} + K_{1,\alpha} C_\alpha \quad (11)$$

$$\beta = K_{0,\beta} + K_{1,\beta} C_\beta \quad (12)$$

$$C_o = C_{o,avg} \Big|_{-2^\circ \leq \alpha \leq +2^\circ, -2^\circ \leq \beta \leq +2^\circ} \quad (13)$$

$$C_q = C_{q,avg} \Big|_{-2^\circ \leq \alpha \leq +2^\circ, -2^\circ \leq \beta \leq +2^\circ} \quad (14)$$

The constants and coefficients $K_{0,\alpha}$, $K_{1,\alpha}$, $K_{0,\beta}$, and $K_{1,\beta}$ are analogous to the same constants and coefficients in the multiple regression model.

The model equations for α and β are best described using figure 7, which shows typical results for C_α versus α for the normal N- and inverted I-roll orientations ($\phi = 0^\circ$ and 180°). Data in this figure were acquired using the abridged test matrix. A figure for the yaw plane data would be very similar to figure 7 except that α would be replaced with β . The discussion below will only refer to the pitch, or α plane, but the discussion is equally valid for the yaw, or β plane. The slope (determined from least-squares linear curve fitting) of the normal curve is $m_{\alpha,N}$ and the slope of the inverted curve is $m_{\alpha,I}$. The actual slope used in the model equation for α is the inverse of the average slope for the two linear curves:

$$K_{1,\alpha} = \frac{2}{m_{\alpha,N} - m_{\alpha,I}} \quad (15)$$

The C_α -intercepts for the linear curves in figure 7 are $b_{\alpha,N}$ and $b_{\alpha,I}$ for the normal and inverted cases, respectively. These are also determined from least-squares linear curve fitting. The corresponding α intercepts are α_N and α_I , the equations for which are

$$\alpha_N = \frac{b_{\alpha,N}}{m_{\alpha,N}} \quad (16)$$

$$\alpha_I = \frac{b_{\alpha,I}}{m_{\alpha,I}} \quad (17)$$

The probe bias angle α_P quantifies asymmetry in the circumferential total pressure ports in the probe head and can be computed using α_N and α_I . The calibration jet flow angle α_F can also be computed from α_N and α_I . Reference 1 gives additional details about deriving α_P and α_F from α_N and α_I . The equations for these two quantities are

$$\alpha_P = \frac{(\alpha_N - \alpha_I)}{2} \quad (18)$$

$$\alpha_F = \frac{(\alpha_N + \alpha_I)}{2} \quad (19)$$

In the discrete linear model, the constant in the α -prediction equation is defined as

$$K_{0,\alpha} = \alpha_P \quad (20)$$

The simple models for C_o and C_q are constant values of C_o and C_q calculated by averaging the C_o and C_q data for α and β angles between $\pm 2^\circ$. The resulting average values are $C_{o,avg}$ and $C_{q,avg}$. As will be shown in the Discussion of Results, the values of C_o and C_q are essentially constant for α and β angles between $\pm 2^\circ$. The constants are only determined using data from the abridged test matrix.

Additional data prediction equations.—Either the multiple regression model or the discrete linear model will predict α , β , C_o , and C_q . When C_o and C_q are known, quantities such as local total pressure, local static pressure, local Mach number, and local velocity can be computed using the following data prediction equations:

$$P_{T,local} = P_5 - C_o(P_5 - P_{6-9,avg}) \quad (21)$$

$$P_{S,local} = P_{T,local} - \frac{(P_5 - P_{6-9,avg})}{C_q} \quad (22)$$

$$M_{local} = \sqrt{\frac{2}{\gamma - 1} \left[\left(\frac{P_{T,local}}{P_{S,local}} \right)^{(\gamma-1)/\gamma} - 1 \right]} \quad (23)$$

$$T_{S,local} = T_{T,local} \left[\left(1 + \frac{\gamma-1}{2} (M_{local})^2 \right)^{-1} \right] \quad (24)$$

$$V_{local} = M_{local} \sqrt{\gamma R T_{S,local}} \quad (25)$$

Note that equations (21) and (22) are just equations (4) and (5) rewritten with $P_{T,local}$ and $P_{S,local}$ on the left-hand side. Equations (23) to (25) are the compressible flow equations for Mach number in terms of a total-to-static-pressure ratio, static temperature in terms of total temperature and Mach number, and velocity in terms of Mach number and the speed of sound. The ratio of specific heats for air is γ and the specific gas constant for air is R .

RESULTS AND DISCUSSION

General Data Trends

Data were acquired for probes 10 and 11 according to the unabridged and abridged test matrices. Typical data for probe 10 at a jet Mach number of 0.6 are found in figures 8 to 13, all of which show data over the $\pm 5^\circ$ α, β -test matrix range. Figure 8 shows the total pressure recovery of pressure port 5 (P_5) compared with the local total pressure $P_{T,local}$. The total pressure recovery is constant at 1.0 for angles α and β between $\pm 2^\circ$. Figure 9 shows the total pressure coefficient C_o ; these data have constant values over a $\pm 2^\circ$ α, β range. Figure 10 shows that the static pressure recovery is constant over a $\pm 2^\circ$ α, β range. The static pressure recovery refers to the recovery of the average static pressure for probe pressure ports 6 to 9 ($P_{6-9,avg}$) compared with the local static pressure $P_{S,local}$. Figure 11 shows the dynamic pressure coefficient C_q data, which are somewhat erratic but can be considered constant for a $\pm 2^\circ$ α, β range. The constant behavior of C_o and C_q over a $\pm 2^\circ$ α, β range is the reason $\pm 2^\circ$ was selected as the α, β range for determining the average constant values of $C_{o,avg}$ and $C_{q,avg}$ to be used in the discrete linear model. Figures 12 and 13 show C_α and C_β over the $\pm 5^\circ$ α, β calibration range. There is no dependence of C_α on β and no dependence of C_β on α . These data validate the assumption in the linear discrete model: α can be predicted accurately without giving any consideration to the value of β and vice versa for a $\pm 5^\circ$ α, β range. All these data trends are typical for all probes.

Comparison of data prediction models.—Using the unabridged test matrix data at $\phi = 0^\circ$ for probes 10 and 11, coefficients were generated for the multiple regression model. The model was then used to predict local values of α , β , C_o , C_q , P_T , P_S , and M over the entire unabridged test matrix using probe pressures from calibration. Using the

abridged test matrix data at $\phi = 0^\circ$, coefficients for the discrete linear model were generated. The discrete linear model was then used to predict local values of α , β , C_o , C_q , P_T , P_S , and M over the entire unabridged test matrix using probe pressures from calibration. The sum of the squared errors between the calibration data and the model prediction data SSE was computed for each model. The results are shown in figures 14 and 15 and are normalized by the sum of the squared differences between the calibration data and the calibration data mean SSD for probes 10 and 11, respectively. The errors are of the same order and indicate that no more error in data prediction is introduced by using the discrete linear model (with coefficients generated using abridged test matrix data) than by using the full third-order multiple regression model (with coefficients generated using unabridged test matrix data). Note that the α and β errors are for the full $\pm 5^\circ$ α, β range whereas the C_o , C_q , P_T , P_S , and M errors are just for a $\pm 2^\circ$ α, β range.

Given these results, it was decided that the linear discrete model would be used for data prediction and that the multiple regression model would not be used because it delivered no more data prediction accuracy. Calibration data acquisition then proceeded according to the abridged test matrix for probes 1 to 9 and 12.

Results using discrete linear model.—In view of the conclusions reached and the decisions made in the previous section, the calibration results will only be presented for the linear discrete model. Additional information such as calibration jet flow angle will be included. The coefficients for all 12 probes and all probe calibration Mach numbers are presented in figures 16 to 21 and are numerically tabulated in the appendix.

Figures 16 and 17 present the discrete linear model slopes, $K_{1,\alpha}$ and $K_{2,\beta}$, respectively for all 12 probes and all calibration Mach numbers. The data show relatively smooth behavior with some slope changes around Mach numbers of 0.4 and 0.5. Because these slopes are rather stable over the Mach number range, there should be no problem using linear interpolation for data prediction at Mach numbers other than those set during calibration.

Figures 18 and 19 show the $K_{0,\alpha}$ and $K_{0,\beta}$ discrete linear model coefficients (probe bias angles, α_p and β_p) for all 12 probes. These angles should be constant for each probe over the Mach number range since α_p and β_p are dictated by pressure port geometric symmetry. The data are essentially constant with a few exceptions, and linear interpolation should satisfactorily yield probe bias angles for Mach numbers other than those set during calibration.

Figures 20 and 21 show the constant values of $C_{o,avg}$ and $C_{q,avg}$ to be used in the linear discrete model for all 12 probes. The $C_{o,avg}$ data generally have values above 0.0 for Mach numbers 0.1 and 0.2 and values below 0.0 for Mach numbers 0.3 and greater. The $C_{q,avg}$ data exhibit similar trends with most of the values being above 1.0 at Mach numbers 0.1 and 0.2 and values below 1.0 for Mach numbers 0.3 and greater. As with all previous calibration coefficients, linear interpolation can be successfully used to predict values of $C_{o,avg}$ for Mach numbers other than those set during calibration.

Figures 22 and 23 present the pitch and yaw jet flow angles for the CE-12 calibration free jet as measured by the 12 individual probes during calibration. The pitch flow angle shows a decreasing trend beginning at about -0.1° for a Mach number of 0.1 and ending at about -0.35° for a Mach number of 0.6. The yaw jet flow angle essentially shows a constant trend at about -0.1° . All the jet flow angle data are negative, which indicates that the jet flow is turning slightly toward the pitch and yaw rotary tables. Figures 1(b), (c), and 2 show the position of the rotary tables with respect to the X,Y,Z-coordinate system and the $+\alpha$ and $+\beta$ directions. This flow turning is probably the result of flow interaction between the jet shear layer and the surrounding ambient air. In addition, the presence and proximity of the rotary tables with respect to the jet must influence this interaction.

Measurement uncertainties.—An analysis was conducted to estimate the uncertainties associated with the linear discrete model coefficients. Additional steps were taken to estimate the uncertainties in flow property predictions when IRT instrumentation is used to acquire probe pressure data. The methodology and nomenclature for the uncertainty analysis follows that presented in reference 3. All instrumentation, apparatus, coefficient, and prediction uncertainties have 95-percent confidence levels.

The starting point for the analysis was to consider the instrumentation and apparatus uncertainties for the CE-12 calibration facility. With these uncertainties quantified (table I), the process of estimating the uncertainties for the discrete linear model coefficients was begun. As previously mentioned, least-squares curve fitting and data averaging were used to obtain values for $K_{0,\alpha}$, $K_{0,\beta}$, $K_{1,\alpha}$, $K_{2,\beta}$, $C_{o,avg}$, and $C_{q,avg}$. After considering the possibility of theoretically estimating the uncertainties associated with the least-squares linear-curve-fit process in conjunction with the uncertainties in table I, it was determined that the most efficient method for estimating the uncertainties in the slopes and intercepts was to do so statistically. Recall that repeat data taken for some probes were used to statistically compute a 95-percent confidence interval on the true slope and a 95-percent confidence interval on the true intercept. The expression for computing the 95-percent confidence interval on the true slope as applied to equation (11) is

$$K_{1,\alpha} \pm t \frac{S_{\alpha,C_\alpha}}{\sqrt{(S_{C_\alpha})^2 (N-1)}} \quad (26)$$

where t is the value from a statistical t -distribution for a 95-percent confidence level and for $N-2$ degrees of freedom; N is the number of data points used in the curve fit; S_{α,C_α} is the standard error of the estimate and is computed by summing the squared α residuals, dividing by $N-2$ degrees of freedom, and taking the square root; S_{C_α} is the standard deviation of the data. The expression for computing the 95-percent confidence interval on the true intercept as applied to equation (11) is

$$K_{0,\alpha} \pm S_{\alpha,C_\alpha} \sqrt{\frac{1}{N} + \frac{(C_{\alpha,avg})^2}{(S_{C_\alpha})^2 (N-1)}} \quad (27)$$

where $C_{\alpha,avg}$ is the average of the C_α data used in the curve fit. The uncertainties in the slopes and intercepts for the pitch plane and yaw plane are identical. For this reason, equations (26) and (27) need only be applied to the pitch plane.

Computing the 95-percent confidence levels for the coefficients $C_{o,avg}$ and $C_{q,avg}$ easily followed from computation of these average coefficients themselves. Along with the averages, standard deviations were computed. These were multiplied by the t -values corresponding to a 95-percent confidence level and for $N-1$ degrees of freedom. Here, N is the number of data points used in computing the standard deviation. The resulting uncertainties in $K_{0,\alpha}$, $K_{0,\beta}$, $K_{1,\alpha}$, $K_{2,\beta}$, $C_{o,avg}$, and $C_{q,avg}$ are given in table II.

As a result of the statistical methods used to determine the uncertainties in the linear discrete model coefficients, the uncertainties in table I were not used explicitly; however, they were used implicitly because the repeat data used in the statistical computations had scatter that directly resulted from the pressure and angular positioning uncertainties given in table I.

With respect to probe calibration, the uncertainties given in table II are all that are necessary. However, it is desirable to know what the uncertainties in α , β , $P_{T,local}$, $P_{S,local}$, M_{local} , and V_{local} will be when the linear discrete model and the additional data prediction equations are used with data acquired in the IRT. The IRT has its own facility instrumentation uncertainties, which are given in table III. No precision error index is given for probe positioning because this is a pure bias error. It is assumed that the pitch-yaw angular position of the probe heads with respect to the IRT test section centerline will be measured with an accuracy of $\pm 0.1^\circ$. Probe head refers to the 5.75-in. length of probe containing the total and static pressure ports.

Arriving at uncertainties in α , β , $P_{T,local}$, $P_{S,local}$, M_{local} , and V_{local} required that the coefficient, instrumentation, and apparatus uncertainties be propagated through equations (11), (12), and (21) to (25). Propagating the uncertainties through these equations was executed according to the methodology described in reference 3 where partial derivatives of each equation were taken with respect to every variable on the right-hand side to produce sensitivity coefficients. Before the partial derivatives were taken, the definitions of C_α , C_β , and $P_{6-9,avg}$ in terms of actual pressures were substituted into the equations. In addition, equations (13) and (14) were substituted into equations (21) and (22). After the sensitivity coefficients had been computed, they were multiplied by the appropriate bias and precision uncertainties and a root-sum-square of the products yielded final uncertainty values for α , β , $P_{T,local}$, $P_{S,local}$, M_{local} , and V_{local} . Uncertainties in γ and R were assumed to be negligible. Bias and precision uncertainties were considered separately but were then combined using the general equation

$$\text{Total uncertainty} = \sqrt{(\text{Bias})^2 + \left[\frac{t(\text{Precision})}{\sqrt{N}} \right]^2} \quad (28)$$

where N is the number of data points that will be averaged to give the result. When data is acquired in the IRT test section, it is anticipated that no fewer than 20 data points will be taken and averaged. Thus, N was set equal to 20. The value for t is selected from a standard statistical t -distribution for a 95-percent confidence level and for $N-1$ degrees of freedom.

The uncertainty results for α , β , $P_{T,local}$, $P_{S,local}$, M_{local} , and V_{local} are given in figures 24(a) to (d). Figure 24(a) shows that the uncertainty in α and β ranges between $\pm 0.46^\circ$ and $\pm 0.12^\circ$ for probe Mach numbers of 0.1 and 0.6, respectively. A comparison of these uncertainty estimates with the 95-percent confidence level for the jet flow angle data in figures 22 and 23 shows reasonable agreement for probe Mach numbers 0.2 and greater. The 95-percent confidence level values for the jet flow angle data were computed by calculating the standard deviation of the data at each probe Mach number in figures 22 and 23 and multiplying by the appropriate t value for 95-percent confidence and 11 degrees of freedom. Poor agreement should be expected at probe Mach numbers approaching 0.0 because the methods described in this section for estimating uncertainty will yield infinite results for probe Mach numbers approaching 0.0. Comparing the estimated uncertainties in flow angle to the 95-percent confidence level of the jet flow angle data is a logical validity check because the jet flow angle data scatter results directly from CE-12 facility instrumentation and apparatus errors. In addition, all 12 probes should have measured the same jet flow angles because the jet flow field remained constant throughout calibration testing.

Figure 24(b) shows the uncertainty in $P_{T,local}$ and $P_{S,local}$. The data indicate that the uncertainty in $P_{T,local}$ will be about ± 0.005 psi at all probe Mach numbers and between ± 0.006 and ± 0.007 psi for $P_{S,local}$. Figures 24(c) and 24(d) show the uncertainty in local Mach number and local velocity. The Mach number uncertainty varies from about ± 0.0037 to ± 0.0007 throughout the probe Mach number range. The velocity uncertainties vary between ± 4.05 and ± 0.80 ft/sec.

CONCLUSIONS

A test program was conducted in the NASA Glenn 3.5-in.-diameter free-jet calibration facility to calibrate 12 new five-hole flow angle pressure probes. The probes will be used in the NASA Glenn Icing Research Tunnel for flow quality surveys and test section calibration. Major conclusions from the test program are given below.

1. General observations of the calibration data revealed constant values of total pressure recovery, static pressure recovery, total pressure coefficient, and dynamic pressure coefficient over a $\pm 2^\circ$ pitch-yaw angle range. Also the pitch angle pressure coefficient showed no dependence on yaw angle and the yaw angle pressure coefficient showed no dependence on pitch angle over the $\pm 5^\circ$ pitch-yaw calibration range.

2. A linear discrete model for predicting pitch angle, yaw angle, total pressure coefficient, and dynamic pressure coefficient was just as accurate as a full third-order multiple regression model. The advantage in using the linear discrete model was that an abridged (sparse) test matrix rather than an unabridged (full) matrix required by the multiple regression model could be used to acquire calibration data.

3. Coefficients were generated for the discrete linear model using least-squares curve fitting and data averaging techniques. Trends in these coefficients revealed relatively smooth behavior such that linear interpolation could be successfully used to arrive at coefficients for probe Mach numbers other than those set during calibration. The slopes for the pitch and yaw angle prediction equations were generally around 12.5° with some decreasing values occurring around probe Mach numbers of 0.4 and 0.5. The intercepts (or probe bias angles) for these pitch and yaw angle prediction equations were generally constant for every probe and typically fell anywhere between $\pm 0.6^\circ$. The average values of total pressure coefficient generally started at about 0.008 for probe Mach numbers of 0.1 and decreased to about -0.002 for Mach numbers of 0.6. The average values of dynamic pressure coefficient generally started at about 1.014 and decreased to values around 0.996 for probe Mach numbers of 0.1 and 0.6, respectively.

4. Uncertainties in the coefficients for the linear discrete model were computed using statistical methods. These uncertainties and Icing Research Tunnel facility instrumentation uncertainties were used to estimate uncertainties in predicted values of pitch angle, yaw angle, local total pressure, local static pressure, local Mach number, and local velocity. When the five-hole probes are used in the IRT test section with IRT facility instrumentation, the uncertainty in both pitch and yaw angle will vary between $\pm 0.46^\circ$ and $\pm 0.11^\circ$ for probe Mach numbers between 0.1 and 0.6, respectively. Uncertainty in total pressure will be about ± 0.005 psi and that in static pressure will be between ± 0.006 and ± 0.007 psi for all probe Mach numbers. The local Mach number uncertainty will vary between ± 0.0037 and ± 0.0007 , and the local velocity uncertainty will vary between ± 4.05 and ± 0.80 ft/sec over the entire probe Mach number range.

5. The linear discrete model coefficients were generated so that pitch and yaw angles could be accurately predicted over a $\pm 5^\circ$ pitch-yaw range. The average total pressure coefficient and dynamic pressure coefficient are only valid over a $\pm 2^\circ$ pitch-yaw range. Thus, predictions in local total pressure, static pressure, Mach number, and velocity should be restricted to a $\pm 2^\circ$ pitch-yaw angle range. It is anticipated that flow angles in the IRT test section will not exceed $\pm 2^\circ$. For this reason, the linear discrete model is more than adequate for predicting local flow properties in this test section.

RECOMMENDATIONS

A new method of holding the two tubular sections during brazing is recommended because the techniques used to braze the two sections together did not always produce the best straightness results. The new method could use a V-block fixture that permits the two tubular sections to be held more accurately along the same axis during brazing.

It may be a good idea to conduct future calibration testing at a Mach number increment smaller than 0.1 to permit better interpolation in the areas where the changes in slope coefficient are more significant, even though the discrete linear model flow angle coefficients were stable enough to apply linear interpolation over the Mach number range.

Use of the multiple regression model is recommended should it be necessary to make flow-field predictions beyond $\pm 2^\circ$ (especially in total pressure and static pressure). Additional calibration data for use with this higher order model should be acquired according to a test matrix similar to the unabridged one. Multiple regression models have been successfully used for flow angles in excess of 30° . The linear discrete model (with calibration data acquired according to the abridged test matrix) proved to be adequate for the small flow angles ($\pm 2^\circ$) expected in the Icing Research Tunnel test section.

APPENDIX—CURVE FIT COEFFICIENTS FOR THE DISCRETE LINEAR MODEL

Probe	Probe Mach number, M_{probe}	Pitch angle slope coefficient, $K_{1,\alpha}$, deg	Pitch probe bias angle coefficient, $K_{0,\alpha}$, deg	Yaw angle slope coefficient, $K_{2,\beta}$, deg	Yaw probe bias angle coefficient, $K_{0,\beta}$, deg	Nondimensional average total pressure coefficient, $C_{p,avg}$	Nondimensional average dynamic pressure coefficient, $C_{q,avg}$
1	0.0996767	12.9575640	-0.2155940	12.8475256	-0.7316980	0.0051180	1.0112873
	.1994736	12.8228144	-.2558100	12.8085254	-.2323790	.0013615	1.0031222
	.2984271	12.5410720	-.2483340	12.6720227	-.2572300	-.0010480	.9973465
	.3981673	11.9958734	-.3114570	11.6829254	-.3516140	-.0013286	.9981720
	.4974697	12.5554007	-.3345710	12.5903357	-.2661810	-.0008536	.9996270
	.5970711	12.4621462	-.3291410	12.3949528	-.2404230	-.0007393	.9988943
2	0.1003453	12.4635441	-0.1424150	12.4758281	-0.2481870	0.0033822	1.0171124
	.1992205	12.3391286	-.1462070	12.3316727	-.2769500	.0016420	1.0012424
	.2980200	12.2511486	-.1045340	12.2367568	-.3666250	-.0027366	.9964535
	.3980644	11.4061502	-.0762530	11.7726005	-.3242670	-.0013338	.9976045
	.4977245	12.2306206	-.1680380	12.0571994	-.3301090	-.0005211	.9984218
	.5964648	12.1038999	-.1836000	12.1872448	-.3625070	-.0010583	.9971829
3	0.1000818	12.7741655	-0.0262270	12.8964032	0.3157010	0.0103898	1.0135002
	.1988733	12.5297582	.0976910	12.7265323	.5646000	.0012580	.9951549
	.2976095	12.2955859	.1612680	12.8445552	.4349920	-.0007696	.9909978
	.3968514	11.8715498	.2812170	12.2286763	.4151340	-.0006733	.9926815
	.4961524	11.4567222	.2024090	11.6114349	.4360610	-.0003588	.9934350
	.5945690	12.1620471	.2006120	12.6175005	.5462980	-.0008454	.9923170
4	0.1002303	12.9252404	-0.0440770	12.6887451	-0.1583590	0.0099798	1.0243292
	.1989662	12.6950274	.0354780	12.5897016	.2604430	.0004606	1.0015645
	.2982242	12.6009652	.0537750	12.4710049	.2653550	-.0025872	.9962485
	.3982419	12.3104195	.1199450	11.6172353	.1139590	-.0015955	.9987959
	.4980270	11.7414992	.1983080	12.5062531	.2564800	-.0010854	1.0002764
	.5977468	12.4635441	-.0867420	12.2924119	.2292810	-.0006710	.9999951
5	0.1001220	12.6704171	-0.3184680	12.5018753	-0.6820590	0.0030055	1.0089558
	.1987851	12.4395129	-.2968260	12.4921924	-.2225330	.0007844	.9979152
	.2977406	12.4593514	-.1464700	12.2709926	-.2113300	-.0016909	.9937285
	.3973075	11.2429029	-.3475990	11.9750440	-.2705020	-.0011550	.9955448
	.4970312	12.3389764	-.2538050	11.8962646	-.2803050	-.0014641	.9957572
	.5963317	12.1065375	-.2790000	12.2393029	-.2608230	-.0011600	.9956055
6	0.0997612	12.6717016	-0.3172420	12.6163862	0.1000660	0.0097547	1.0133146
	.1987291	12.4334809	-.1599710	12.5106340	.4245670	.0004970	.9946786
	.2976096	12.5070352	-.0500220	12.3632318	.3649730	-.0020700	.9922684
	.3971147	11.8759204	-.0199220	11.7568219	.3516470	-.0015849	.9936034
	.4970837	11.7352986	-.1387850	12.2868236	.4296700	-.0008754	.9955465
	.5956371	12.2312190	.0223950	12.1549513	.3948340	-.0009793	.9945269

Probe	Probe Mach number, M_{probe}	Pitch angle slope coefficient, $K_{1,\alpha}$, deg	Pitch probe bias angle coefficient, $K_{0,\alpha}$, deg	Yaw angle slope coefficient, $K_{2,\beta}$, deg	Yaw probe bias angle coefficient, $K_{0,\beta}$, deg	Nondimensional average total pressure coefficient, $C_{0,avg}$	Nondimensional average dynamic pressure coefficient, $C_{q,avg}$
7	0.0997271	12.8587594	-0.2409030	12.9407959	0.6509910	0.0022983	1.0107034
	.1991722	12.6159087	-.0853030	12.6680095	.5919660	.0007784	1.0006593
	.2979321	12.6070019	.0940290	12.7000254	.4686520	-.0001801	.9959084
	.3976125	12.2342118	-.0009770	12.0470316	.4290650	-.0000857	.9972521
	.4969901	12.1216529	-.1938710	11.8973969	.5169140	-.0001535	.9974650
	.5961985	12.2476974	-.0063770	12.4252929	.4824580	-.0002569	.9965313
8	0.1003990	12.5661293	0.0590940	12.5380844	-0.2047690	0.0014989	1.0142827
	.1989827	12.4886042	.2479680	12.5154879	-.2691520	.0014516	.9999390
	.2983054	12.4480295	.2448880	12.5478386	-.2064940	-.0004112	.9966141
	.3977217	11.5665772	.2563970	12.0281941	-.2045950	.0002662	.9974975
	.4975920	12.1704841	.2583910	11.6588164	-.2862400	.0002078	.9989809
	.5966901	12.0815261	.2804150	12.2068822	-.2601420	-.0003920	.9979311
9	0.1002158	12.7338249	-0.4308310	12.6905164	0.6197570	0.0105245	1.0177346
	.1992464	12.4621462	-.3991520	12.5528790	.4289720	.0022194	1.0001847
	.2984083	12.4235949	-.4011210	12.6186150	.4178910	.0004991	.9987478
	.3981932	11.9341711	-.4141480	12.1018492	.4039940	.0008093	.9998224
	.4978641	11.9428653	-.3836140	11.6384628	.5466100	-.0001588	.9996819
	.5969999	12.4229775	-.4327410	12.2490476	.4615950	-.0005303	.9984810
10	0.0997254	12.7026066	-0.4584000	12.6847213	0.1887070	0.0087438	1.0160140
	.1991652	12.5281884	-.4112500	12.5572927	.0841070	.0007939	1.0005794
	.2981026	12.4840828	-.3268780	12.3334978	.1067270	.0004924	.9964912
	.3973918	11.9587185	-.3125680	11.6907106	.0264670	.0000642	.9967415
	.4968086	12.0037932	-.3915520	12.1132834	.0350740	-.0002164	.9968923
	.5965865	12.1796746	-.3528960	12.1969069	.1125430	-.0004063	.9961092
11	0.0993741	13.2860351	-0.4485310	13.4424863	-0.1152040	0.0028607	1.0071670
	.1989469	13.2304883	-.4008270	13.2911561	-.3532430	.0013865	1.0018344
	.2983377	13.0821559	-.2709480	13.1040990	-.3014470	.0002459	.9981764
	.3982296	12.1241513	-.4854330	12.2898437	-.4133400	.0003327	.9988014
	.4975064	12.8382889	-.3291300	12.8389482	-.3501400	-.0000829	.9986042
	.5969402	12.6881011	-.2389170	12.9292511	-.2976750	-.0003286	.9980231
12	0.0997374	12.8282427	0.2721910	12.7792261	-0.2322230	0.0094311	1.0144519
	.1991558	12.6328023	.2613110	12.5979491	-.2805080	.0017933	1.0007789
	.2980667	12.7090641	.2133310	12.5634454	-.2631320	.0004732	.9968901
	.3975640	12.1908106	.2561070	11.9425801	-.3345780	.0002680	.9967369
	.4973765	11.5170222	.2802820	12.1679666	-.3806420	.0000265	.9979215
	.5964044	12.2652733	.2413980	12.3943383	-.3352120	-.0004728	.9968171

REFERENCES

1. Clark, E.L.; Henfling, J.F.; and Aeschliman, D.P.: Calibration of Hemispherical-Head Flow Angularity Probes. AIAA Paper 92-4005, July 1992.
2. Everett, K.N.; Gerner, A.A.; and Durston, D.A.: Seven-Hole Cone Probes for High Angle Flow Measurement: Theory and Calibration. AIAA J., vol. 21, no. 7, July 1983, pp. 992-998.
3. Coleman, H.W.; and Steele, W.G.: Experimentation and Uncertainty Analysis for Engineers. John Wiley & Sons, Inc., New York, 1989.

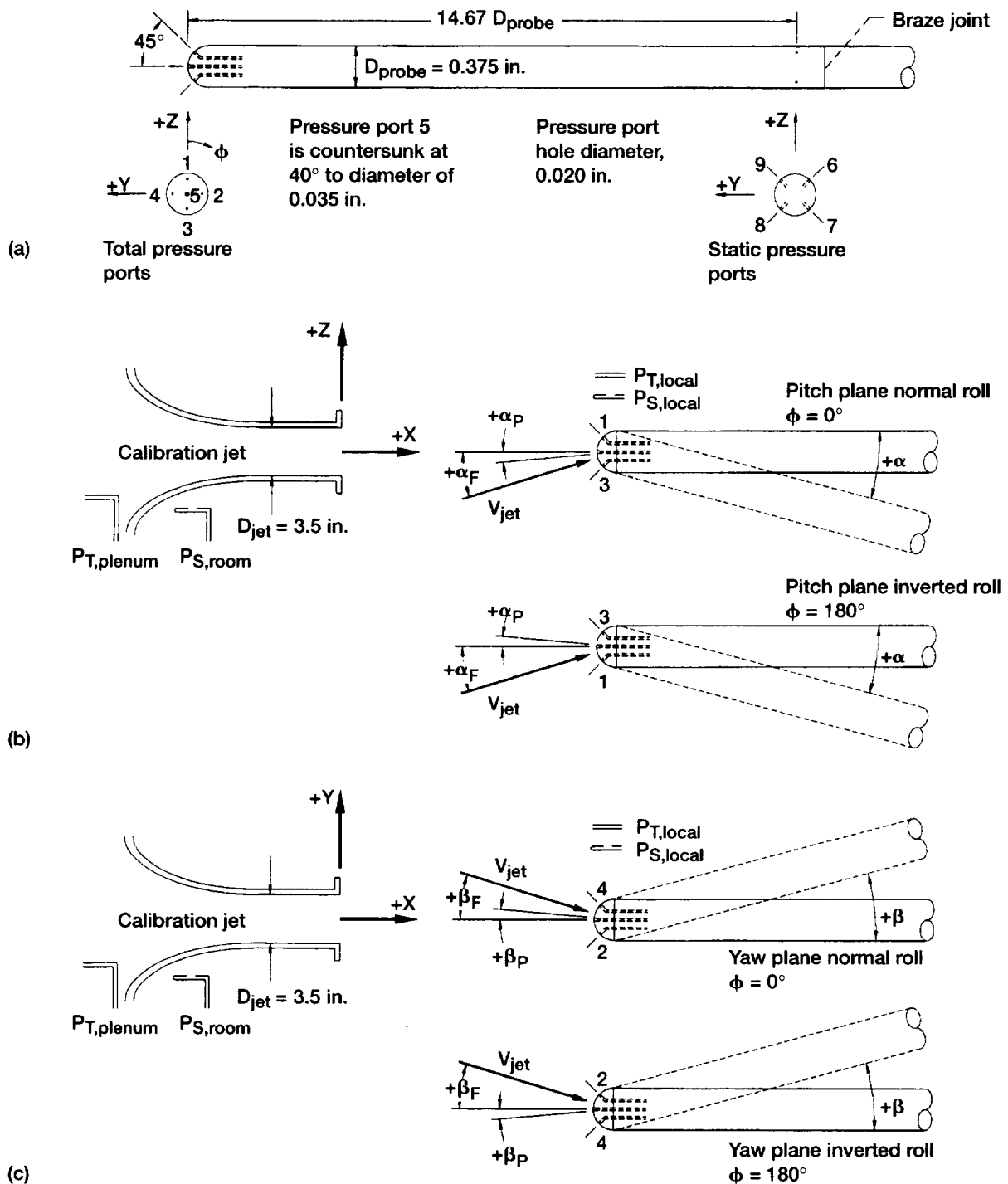


Figure 1.—Five-hole probe. (a) Icing Research Tunnel (IRT) probe design and pressure port identification. (b) Calibration nomenclature for pitch plane in normal- and inverted-roll orientations. (c) Calibration nomenclature for yaw plane in normal- and inverted-roll orientations.

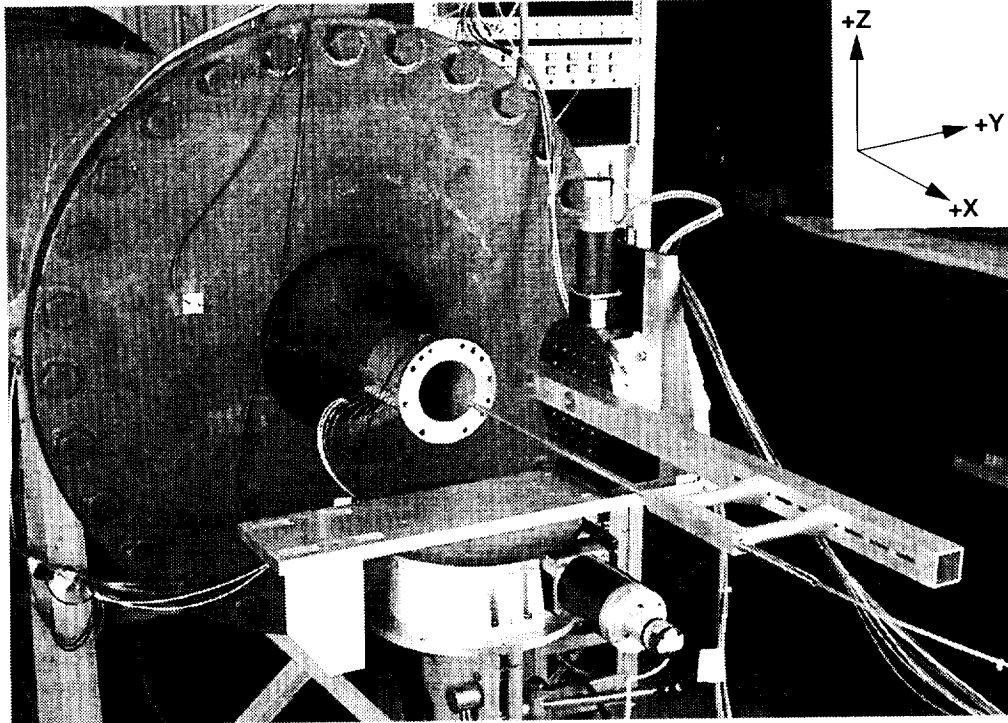


Figure 2.—IRT five-hole probe calibration test setup in NASA Glenn 3.5-in.-diameter free-jet calibration facility (CE-12). Vertical rotary table in pitch plane; horizontal rotary table in yaw plane; X, Y, Z-coordinate axes are shown displaced from jet exit.

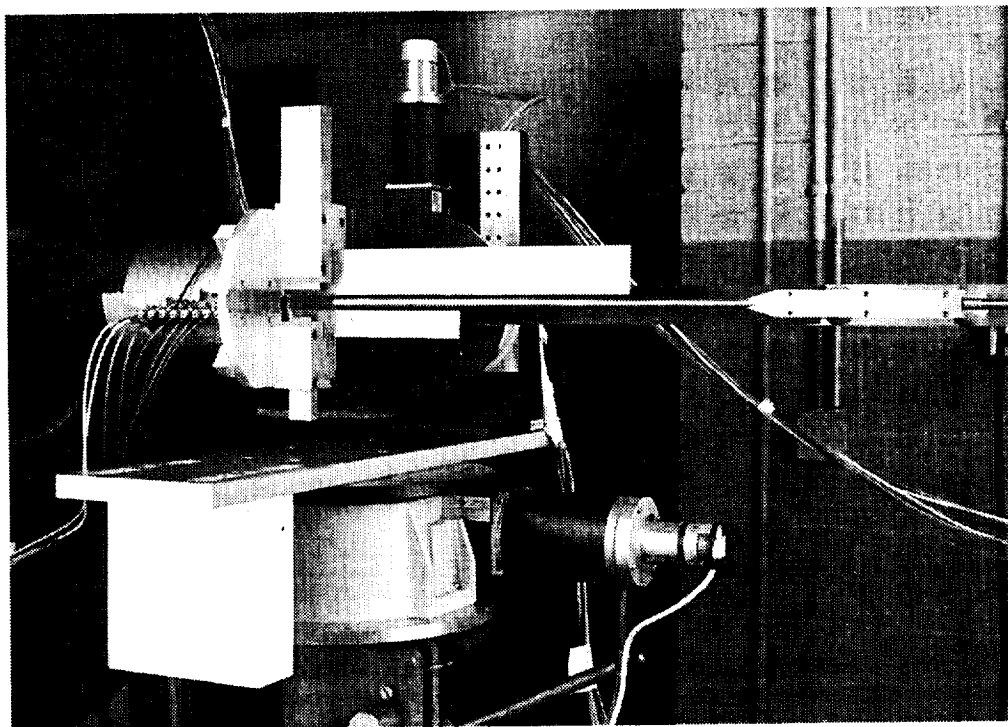


Figure 3.—IRT five-hole probe alignment technique using CE-12 alignment fixture.

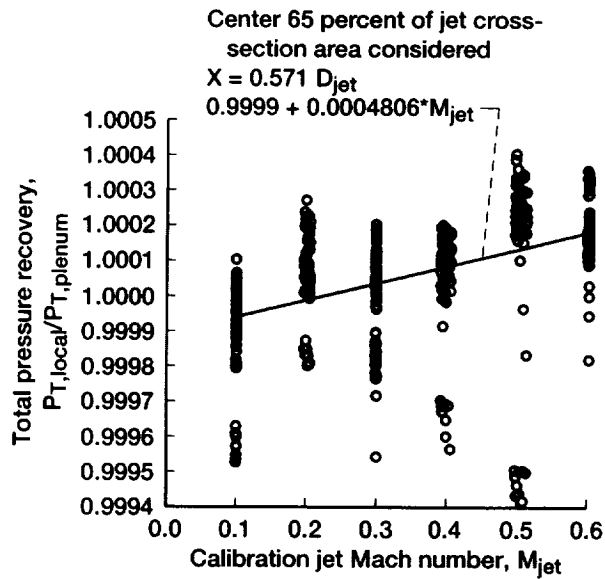


Figure 4.—Total pressure recovery for CE-12 calibration free jet as measured by total pressure rake downstream of jet exit.

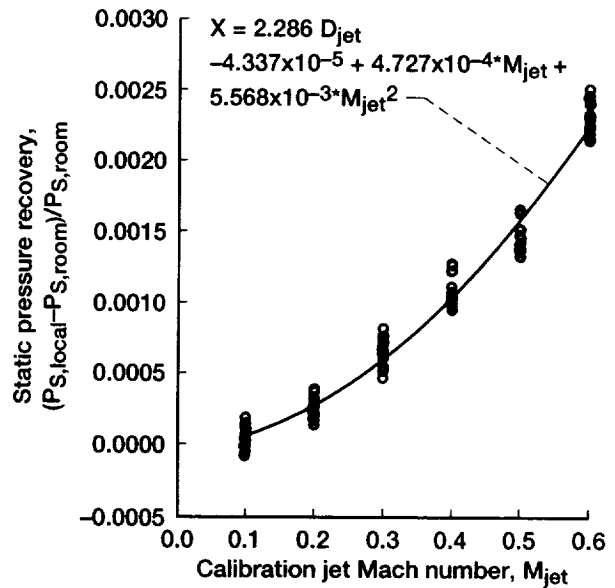


Figure 5.—Static pressure recovery for CE-12 calibration free jet as measured by centerline static pressure probe downstream of jet exit.

- Unabridged test matrix, normal roll, $\phi = 0^\circ$
- Unabridged test matrix, inverted roll, $\phi = 180^\circ$
- △ Abridged test matrix, normal roll, $\phi = 0^\circ$
- ◇ Abridged test matrix, inverted roll, $\phi = 180^\circ$

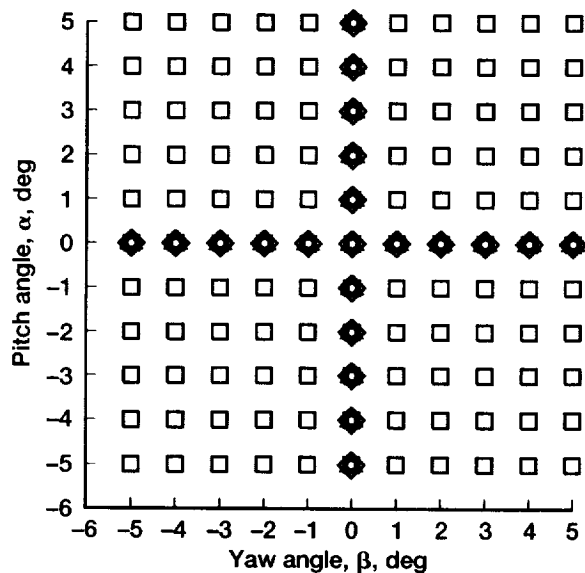


Figure 6.—Unabridged and abridged test matrices for IRT five-hole probe calibration data acquisition. $M_{jet} = 0.1, 0.2, 0.3, 0.4, 0.5, 0.6$.

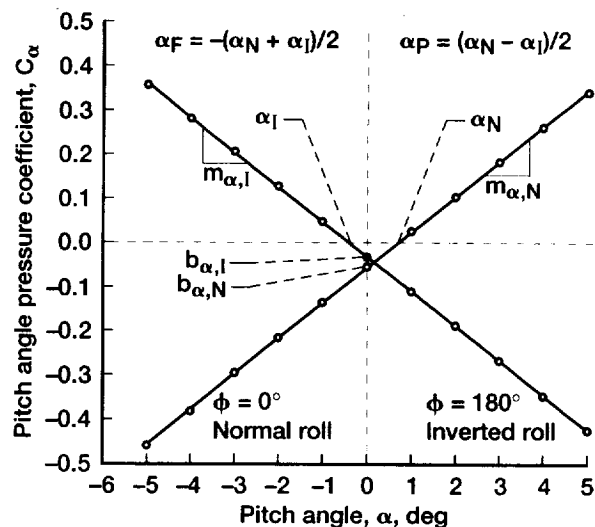


Figure 7.—Typical data for C_{α} versus α for normal and inverted-roll orientations (nomenclature for discrete linear model is defined in text in symbols section).

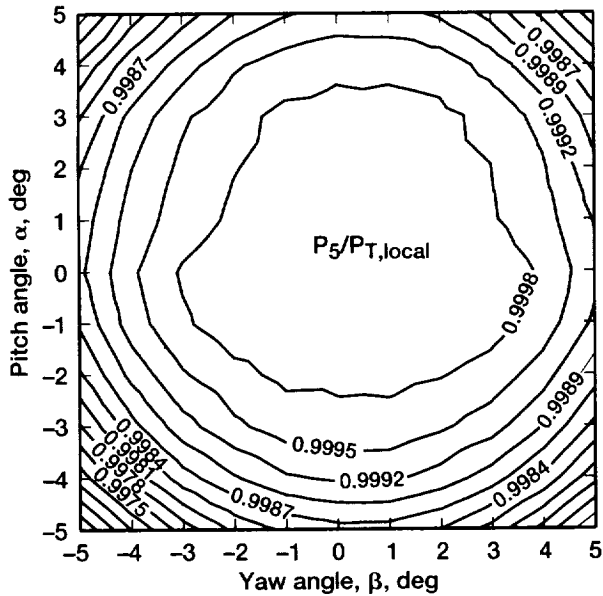


Figure 8.—Total pressure recovery for total pressure port 5 on probe 10 at $M_{\text{probe}} = 0.6$. Data acquired according to unabridged test matrix at $\phi = 0^\circ$ and are typical for all probes.

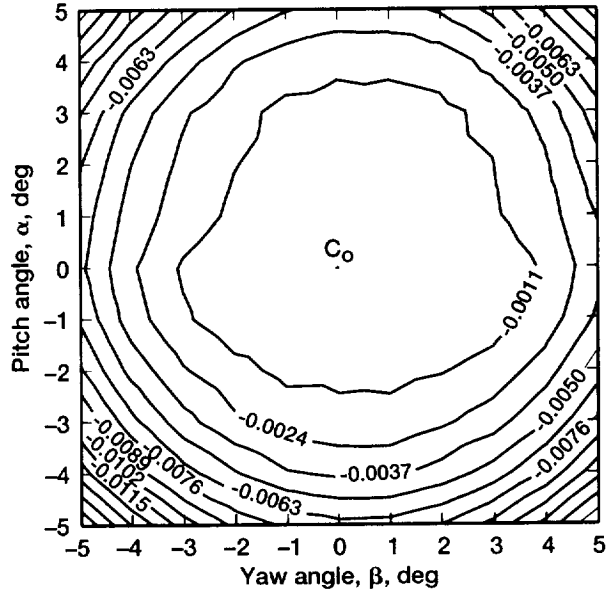


Figure 9.—Total pressure coefficient for probe 10 at $M_{\text{probe}} = 0.6$. Data were acquired according to unabridged test matrix at $\phi = 0^\circ$ and are typical for all probes.

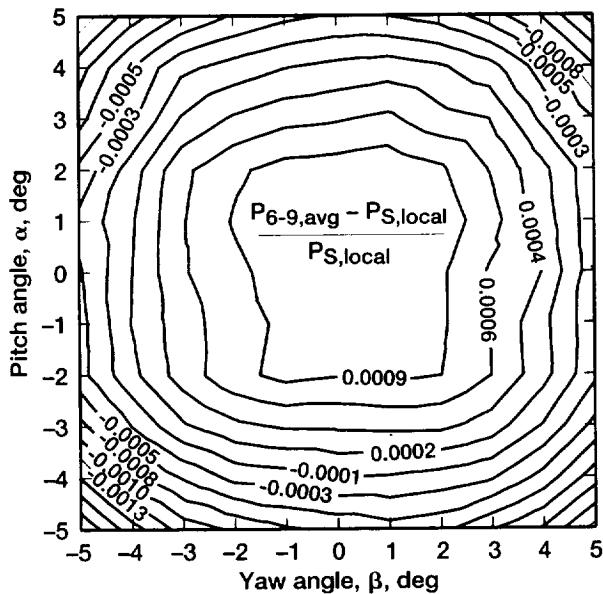


Figure 10.—Static pressure recovery for static pressure ports 6 to 9 on probe 10 at $M_{\text{probe}} = 0.6$. Data were acquired according to unabridged test matrix at $\phi = 0^\circ$ and are typical for all probes.

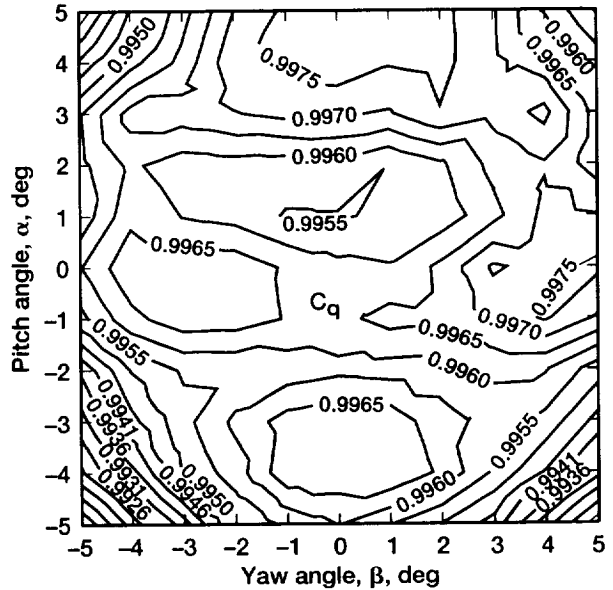


Figure 11.—Dynamic pressure coefficient for probe 10 at $M_{\text{probe}} = 0.6$. These data were acquired according to unabridged test matrix at $\phi = 0^\circ$ and are typical for all probes.

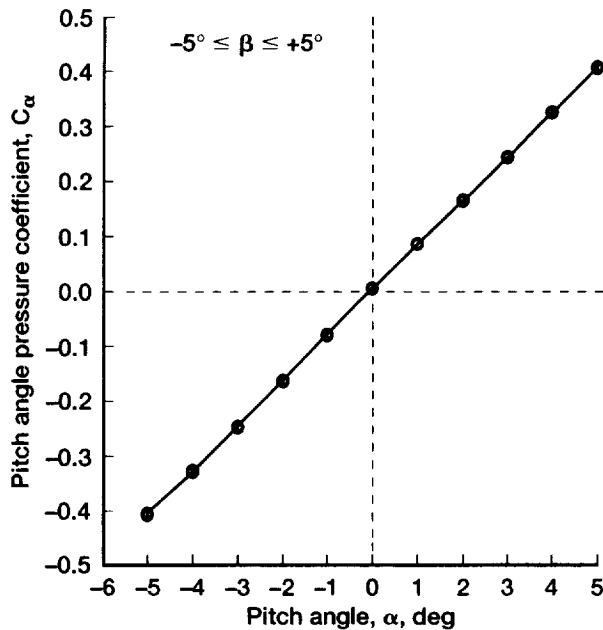


Figure 12.—Data for C_{α} versus α for probe 10 at $M_{\text{probe}} = 0.6$. Data were acquired according to unabridged test matrix at $\phi = 0^\circ$ and are typical for all probes.

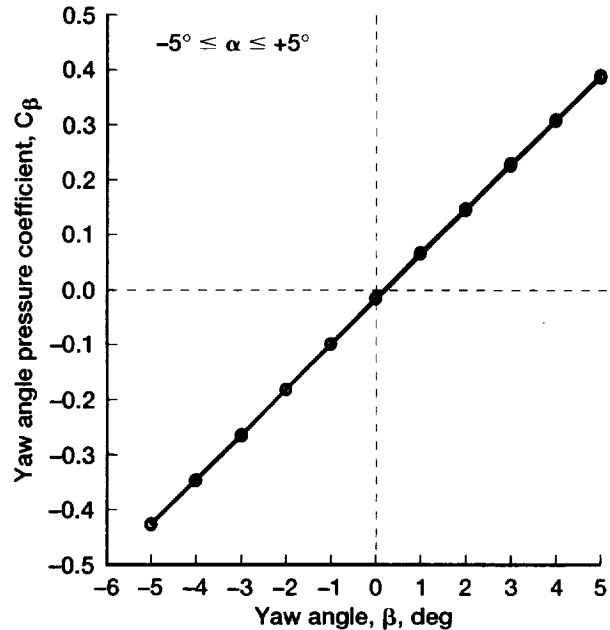


Figure 13.—Data for C_{β} versus β for probe 10 at $M_{\text{probe}} = 0.6$. Data were acquired according to unabridged test matrix at $\phi = 0^\circ$ and are typical for all probes.

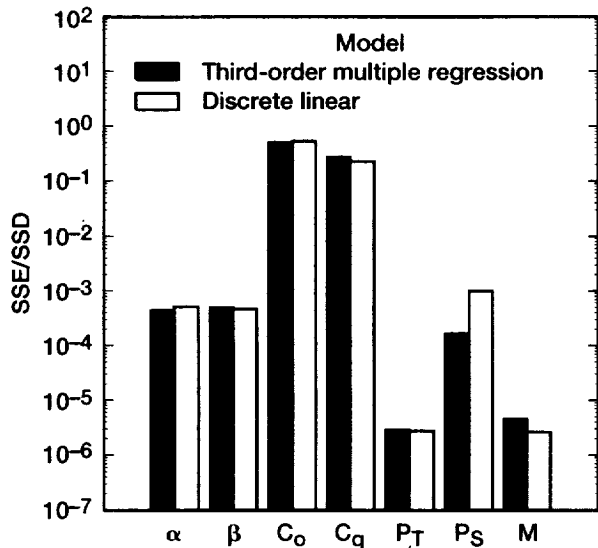


Figure 14.—Sum of squared errors between calibration data and model prediction data normalized by sum of squared differences between calibration data and calibration data mean for probe 10. Models used were third-order multiple regression and discrete linear.

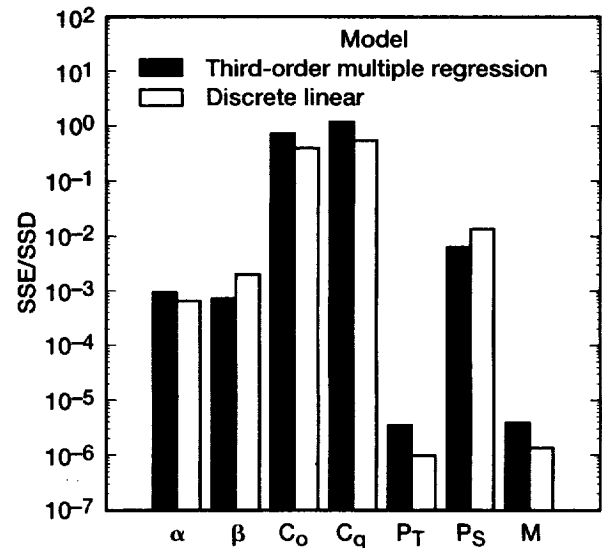


Figure 15.—Sum of squared errors between calibration data and model prediction data normalized by sum of squared differences between calibration data and calibration data mean for probe 11. Models used were third-order multiple regression and discrete linear.

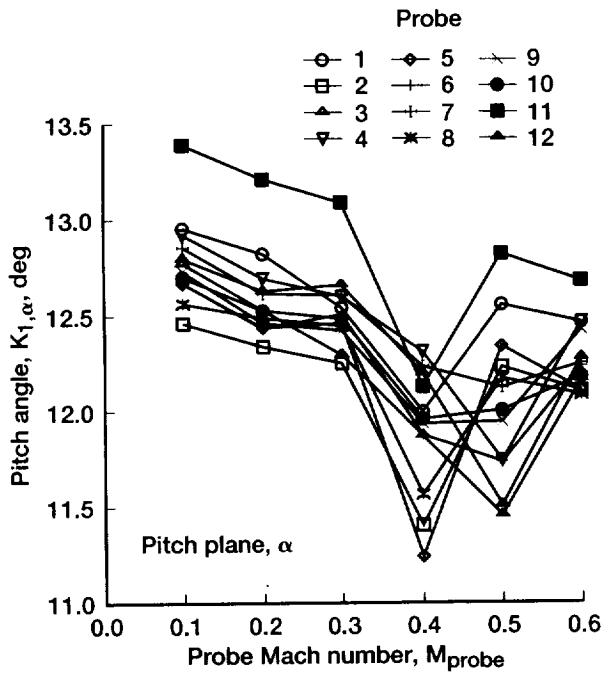


Figure 16.—Slopes of pitch angle $K_{1,\alpha}$ calibration curves to be used with linear discrete model for all 12 probes.

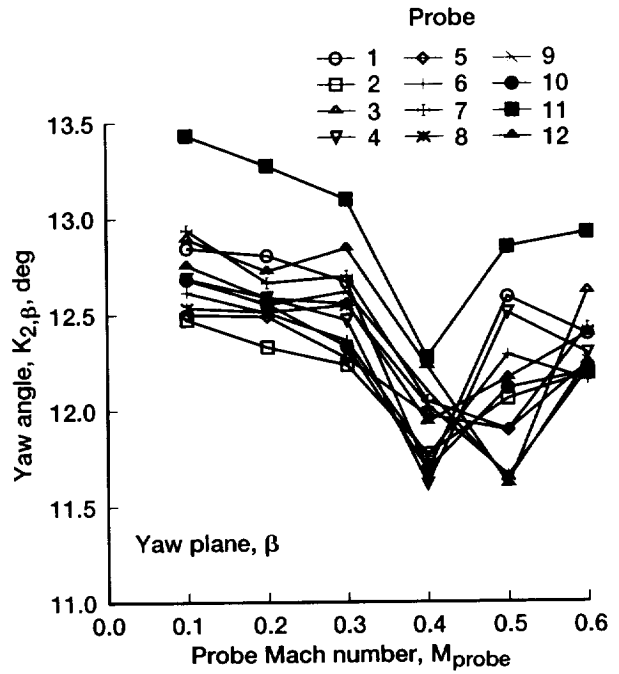


Figure 17.—Slopes of yaw angle $K_{2,\beta}$ calibration curves to be used with linear discrete model for all 12 probes.

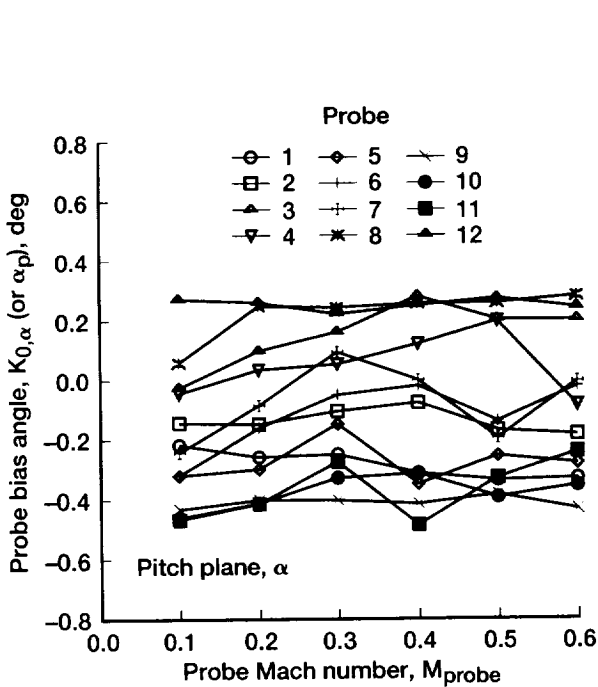


Figure 18.—Probe bias angles $K_{0,\alpha}$ (or α_p) for pitch angle calibration curves to be used with linear discrete model for all 12 probes.

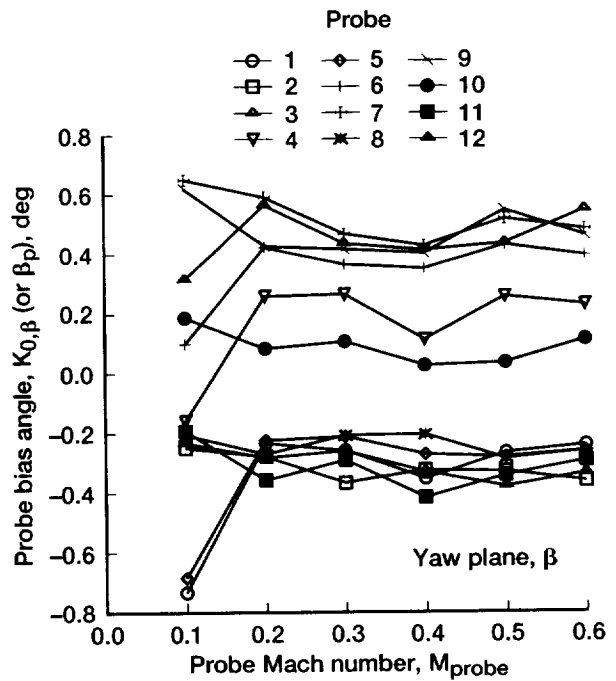


Figure 19.—Probe bias angles $K_{0,\beta}$ (or β_p) for yaw angle calibration curves to be used with linear discrete model for all 12 probes.

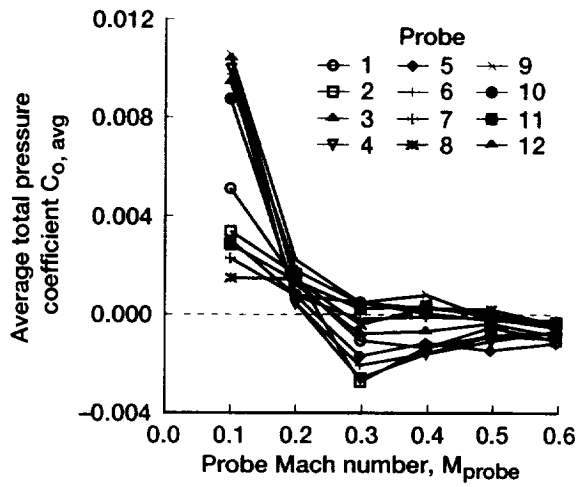


Figure 20.—Average total pressure coefficient $C_{o,avg}$ constants for all 12 probes to be used with linear discrete model.

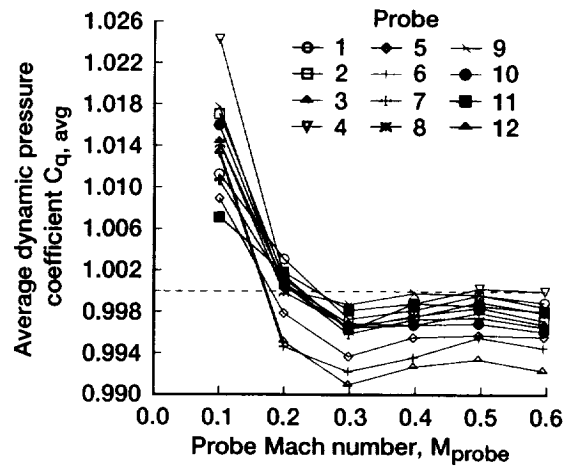


Figure 21.—Average dynamic pressure coefficient $C_{q,avg}$ constants for all 12 probes to be used with linear discrete model.

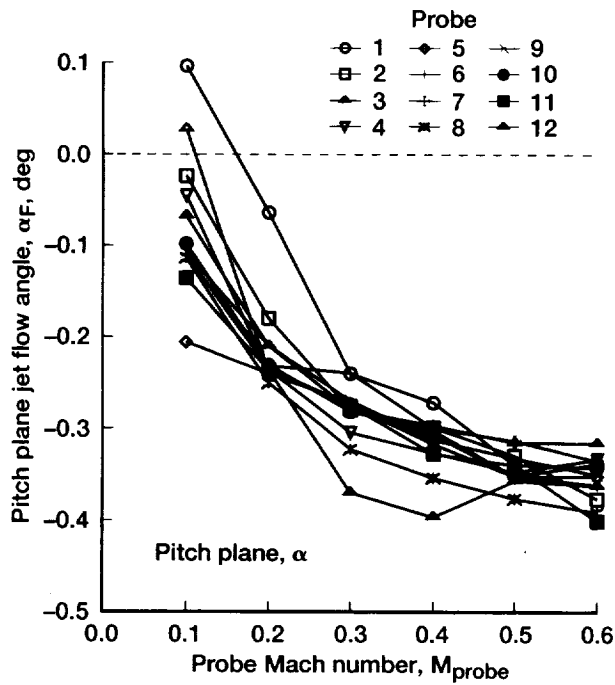


Figure 22.—CE-12 jet flow angle in pitch plane α_F as measured by all 12 probes.

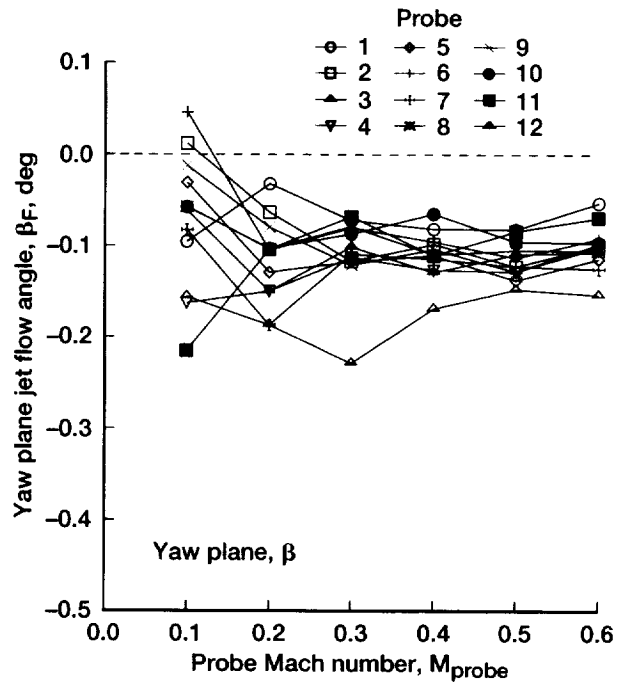


Figure 23.—CE-12 jet flow angle in yaw plane β_F as measured by all 12 probes.

REPORT DOCUMENTATION PAGEForm Approved
OMB No. 0704-0188

Public reporting burden for this collection of information is estimated to average 1 hour per response, including the time for reviewing instructions, searching existing data sources, gathering and maintaining the data needed, and completing and reviewing the collection of information. Send comments regarding this burden estimate or any other aspect of this collection of information, including suggestions for reducing this burden, to Washington Headquarters Services, Directorate for Information Operations and Reports, 1215 Jefferson Davis Highway, Suite 1204, Arlington, VA 22202-4302, and to the Office of Management and Budget, Paperwork Reduction Project (0704-0188), Washington, DC 20503.

1. AGENCY USE ONLY (Leave blank)		2. REPORT DATE May 1999	3. REPORT TYPE AND DATES COVERED Final Contractor Report	
4. TITLE AND SUBTITLE Five-Hole Flow Angle Probe Calibration for the NASA Glenn Icing Research Tunnel			5. FUNDING NUMBERS WU-523-91-13-00 NAS3-27186	
6. AUTHOR(S) Jose C. Gonzalez and E. Allen Arrington				
7. PERFORMING ORGANIZATION NAME(S) AND ADDRESS(ES) Dynacs Engineering Company, Inc. 2001 Aerospace Parkway Brook Park, Ohio 44142			8. PERFORMING ORGANIZATION REPORT NUMBER E-10677	
9. SPONSORING/MONITORING AGENCY NAME(S) AND ADDRESS(ES) National Aeronautics and Space Administration John H. Glenn Research Center at Lewis Field Cleveland, Ohio 44135-3191			10. SPONSORING/MONITORING AGENCY REPORT NUMBER NASA CR-1999-202330 AIAA-96-2201	
11. SUPPLEMENTARY NOTES Prepared for the 19th Advanced Measurement and Ground Testing Technology Conference sponsored by the American Institute of Aeronautics and Astronautics, New Orleans, Louisiana, June 17-20, 1996. Project Manager, Sandra L. Hardy, Facilities and Test Engineering Division, NASA Glenn Research Center, organization code 7560, (216) 433-2278.				
12a. DISTRIBUTION/AVAILABILITY STATEMENT Unclassified - Unlimited Subject Categories: 01 and 09 Distribution: Nonstandard This publication is available from the NASA Center for AeroSpace Information, (301) 621-0390.			12b. DISTRIBUTION CODE	
13. ABSTRACT (Maximum 200 words) A spring 1997 test section calibration program is scheduled for the NASA Glenn Research Center Icing Research Tunnel following the installation of new water injecting spray bars. A set of new five-hole flow angle pressure probes was fabricated to properly calibrate the test section for total pressure, static pressure, and flow angle. The probes have nine pressure ports: five total pressure ports on a hemispherical head and four static pressure ports located 14.7 diameters downstream of the head. The probes were calibrated in the NASA Glenn 3.5-in.-diameter free-jet calibration facility. After completing calibration data acquisition for two probes, two data prediction models were evaluated. Prediction errors from a linear discrete model proved to be no worse than those from a full third-order multiple regression model. The linear discrete model only required calibration data acquisition according to an abridged test matrix, thus saving considerable time and financial resources over the multiple regression model that required calibration data acquisition according to a more extensive test matrix. Uncertainties in calibration coefficients and predicted values of flow angle, total pressure, static pressure, Mach number, and velocity were examined. These uncertainties consider the instrumentation that will be available in the Icing Research Tunnel for future test section calibration testing.				
14. SUBJECT TERMS Flow angle probe; Probe calibration; Wind tunnel; Icing research; Free jet; Uncertainty			15. NUMBER OF PAGES 29	
			16. PRICE CODE A03	
17. SECURITY CLASSIFICATION OF REPORT Unclassified	18. SECURITY CLASSIFICATION OF THIS PAGE Unclassified	19. SECURITY CLASSIFICATION OF ABSTRACT Unclassified	20. LIMITATION OF ABSTRACT	

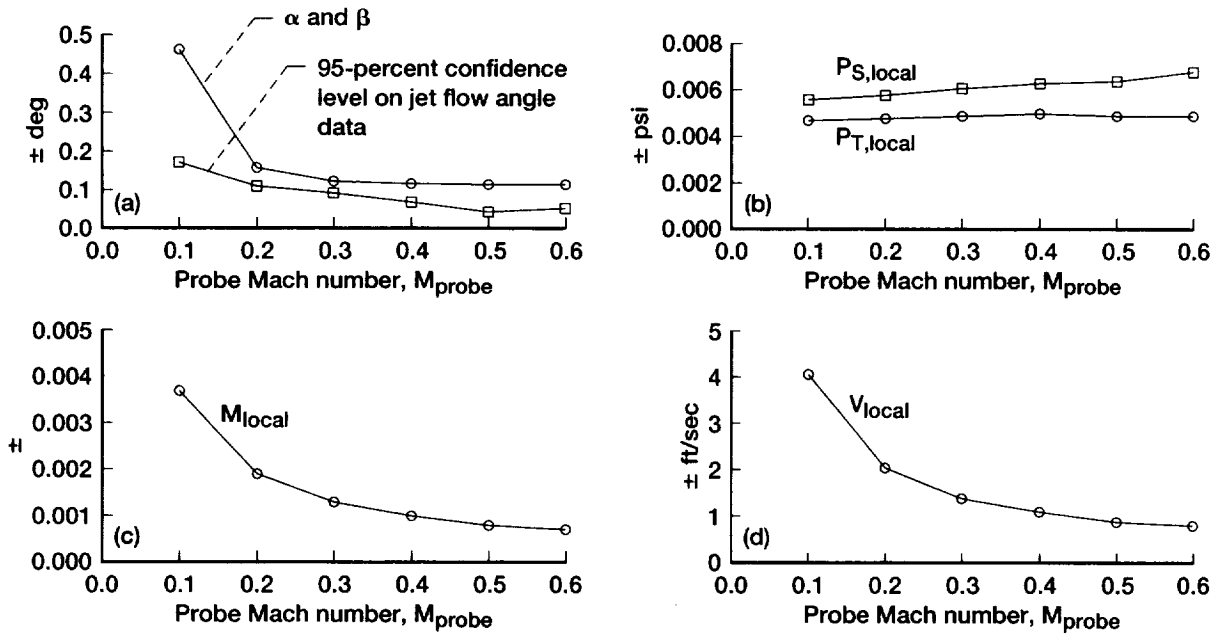


Figure 24.—Uncertainties in (a) pitch and yaw angle, (b) local total pressure and local static pressure, (c) local Mach number, and (d) local velocity for discrete linear model data prediction equations used in conjunction with data acquired in Icing Research Tunnel.